Using CFD to improve the irrigation strategy for growing ornamental plants inside a greenhouse

Hacene Bouhoun Ali, Pierre-Emmanuel Bournet, Patrice Cannavo, Etienne E. Chantoiseau

Hacene Bouhoun Ali, Pierre-Emmanuel Bournet, Patrice Cannavo, Etienne E. Chantoiseau. Using CFD to improve the irrigation strategy for growing ornamental plants inside a greenhouse. Biosystems Engineering, 2019, 186, pp.130-145. 10.1016/j.biosystemseng.2019.06.021 . hal-02271272

Version of Record: https://www.sciencedirect.com/science/article/pii/S1537511018310432
Manuscript_eda3878b8b4bffe660ab045d45cec62b

Using CFD to improve the irrigation strategy for growing ornamental plants inside a greenhouse.

Hacene Bouhoun Ali[1], Pierre-Emmanuel Bournet[1*], Patrice Cannavo[1], Etienne Chantoiseau[1]

[1] EPHor, AGROCAMPUS OUEST, 49045 Angers, France

E-mail: Pierre-Emmanuel.Bournet@agrocampus-ouest.fr

Tel: +33 (0)2 41 22 55 04; Fax: +33 (0)2 41 22 55 53

Abstract

In order to cope with water scarcity, improved water management should be implemented to reduce water inputs without affecting production. A better quantifying of the heat and water vapour transfers in response to water restriction is thus needed. Distributed climate models, with the addition of transfers through the substrate-plant-atmosphere continuum calculation is a useful tool. However, such models have generally been established for plants grown in well-watered conditions. This study aimed to simulate the transpiration of plants grown in pots and the resulting microclimate in a greenhouse compartment under different irrigation regimes. An experiment was conducted on New Guinea impatiens grown in containers on shelves, in a 100-m^2 greenhouse compartment. A 2D transient CFD model was implemented, including a specific sub-model taking into account the water transport in the substrate-plant-atmosphere continuum, as well as the resulting crop interactions with the greenhouse climate for both well-watered and restricted water conditions. The substrate water content was calculated from the water balance. Special care was paid to model the stomatal resistance. Simulation results showed the model ability to correctly predict transpiration, air and leaf temperatures, as well

---

[*] Corresponding author

as greenhouse air humidity for both irrigation conditions. Different irrigation scenarios were then tested by reducing the water supply from 100 to 50 % of the substrate retention capacity. Simulations allow assessing the model responses on plant transpiration, growing media water potential and climate distribution inside the greenhouse. Consequently, the CFD model could be useful to define an irrigation strategy for a better water input management.

Keywords: Crop model, irrigation, matric potential, Penman-Monteith equation, stomatal resistance, unsteady-state conditions, greenhouse.

Nomenclature

C_D	Drag coefficient
C_F	Non-linear momentum loss coefficient
C_p	Specific heat of air, J kg^{-1} K^{-1}
CTR	Cumulated transpiration ratio
$\mathrm{D}_{ref,j}$	Difference between the considered irrigation case *j* and the reference case
H	Plant height, m
Kc	Extinction coefficient for solar radiation
k	Turbulent kinetic energy, m^2 s^{-2}
LAD	Leaf area density, m^2 m^{-3}
M	Molecular weight of species, kg mol^{-1}
N	Dimensionless parameter
P	Pressure, Pa
Q_s	Sensible heat flux density, W m^{-3}
R_a	Leaf aerodynamic resistance, s m^{-1}
R	Universal gas constant, J Mol^{-1} K^{-1}
rg	Reduced global radiation

Rg_0	Above-canopy global radiation, W m^{-2}
Rg	Global radiation
rh	Reduced relative air humidity
RH	Relative air humidity, %
$RMSE$	Root mean square error
Rn	Net radiation, W m^{-2}
$r_{s,min}$	Minimal leaf stomatal resistance, s m^{-1}
R_s	Leaf stomatal resistance, s m^{-1}
$\mathrm{s_s}$	Total area of shelves, m^2
S_Φ	Source term
ts	Time step interval, s
T	Temperature, K
Tr_d	Latent heat flux density, W m^{-3}
U, V	Components of the velocity vector, m s^{-1}
VPD	Vapour pressure deficit, Pa
y	Variable
α	Parameter, kPa^{-1}
γ	Psychrometric constant, Pa K^{-1}
Δ	Slope of the saturated water vapour pressure curve, Pa K^{-1}
ε	Dissipation rate, m^2 s^{-3}
θ	Volumetric water content, v/v
λ	Water latent heat of vaporisation, kJ kg^{-1}
Γ	Diffusion coefficient, Kg m^{-1} s^{-1}
μ	Dynamic viscosity, kg m^{-1} s^{-1}

ρ	Density, kg m^{-3}
τ	Reduced temperature
Φ	Concentration of transported quantity
Ψ	Peat matric potential, kPa
ω	Mass fraction

Subscripts

a	Air
e	East
abs	Absorbed
atm	Atmospheric
avg	Volume-weighted average
c	Well-watered
w_g	Ground
l	Leaf
out	*Outside*
PAR	Photosynthetically active radiation
r	Water restriction
res	Residual
sc	Screen
sat	Saturation
sky	Sky
w	Water
w	West

1 INTRODUCTION

Reducing water consumption in greenhouses by increasing the efficiency of its use is of prime interest, not only for environmental reasons but also for economic ones. In order to better manage water resources, it is necessary to develop adapted strategies. Currently, the question of an optimal control of irrigation for ornamental crops grown in greenhouses has not been investigated to the same extent as it has been for open field crops. The aim is thus to reduce the water consumption of the plants without significantly impacting their transpiration and growth rate. The response of plants to different irrigation regimes could be assessed using a modelling approach. The key factor that controls transpiration is stomatal resistance, which is a function of the stomatal aperture that decreases with reduced irrigation, impacting not only transpiration but CO_2 absorption for photosynthesis as well and, consequently, plant growth. A compromise must therefore be found between transpiration and photosynthesis to cope with the contradiction between a lower transpiration rate for an optimal management of water resources, and the expected vegetative development resulting from photosynthetic activity (Monteith, 1977). Furthermore, transpiration cools the leaves and impacts the distribution of several climatic variables in the vicinity of the plants, such as temperature and humidity (Kichah, Bournet, Migeon, & Boulard, 2012).

Computational fluid dynamics (CFD) is a powerful tool that makes it possible to predict the distribution of the climatic variables inside a greenhouse and to test different configurations without incurring high costs. Modelling the microclimate and transpiration rate distribution under greenhouse conditions has been extensively investigated through CFD tools (Boulard & Wang, 2002; Majdoubi, Boulard, Fatnassi, & Bouirden, 2009; Nebbali, Roy, & Boulard, 2012) but only for well-watered conditions. A recent study of (Bouhoun Ali, Bournet, Cannavo, & Chantoiseau, 2018) considered the case of water restriction, but calculations were only applied to a limited domain (23× 3.69 m^2) around the plants. To date, there is no CFD study that simulates restricted water conditions and their impact on microclimate and plant transpiration at the greenhouse scale.

The objective of this study was to implement an accurate unsteady 2D CFD model at the greenhouse scale to simulate the water transfer in the substrate-plant-atmosphere continuum and the microclimate distribution inside a greenhouse for different irrigation regimes.

In the first stage, the model was validated against data recorded inside a greenhouse compartment containing a New Guinea impatiens crop both for well-watered and restricted water conditions. A series of irrigation scenarios was then tested to assess the behaviour of the plants in response to water restrictions together with the microclimate generated mainly in the vicinity of the plants, and to suggest recommendations to reduce water inputs without significantly impacting on plant transpiration.

2 MATERIALS AND METHODS

2.1 Experimental device

2.1.1 Experimental setup

Experiments took place in Angers in north-western France (47°28’ N, 0°33’ E) in 2014, inside a 100-m^2 Venlo glasshouse compartment (CMF Group, Varades, France) that was part of a larger greenhouse (~3000 m^2) and that was separated from the adjacent compartments by glass walls. The compartment (gutter height: 3.9 m; ridge height: 5.9 m) was covered with a 4-mm thick horticultural glass and equipped with continuous roof vents on both ridge sides that were opened during the day and closed at night. In order to avoid excessive temperatures, a shade screen was used and the roof vents were fully opened as soon as external temperatures exceeded 20°C. Inside the greenhouse, young Impatiens plants (Novae-Guinea, cv. ‘Sonic Scarlet’) were grown on shelves and potted in 0.74 l containers (height: 87 mm) filled with fine peat (particle size: 0-2 mm) with homogeneous peat bulk density (i.e., 120 kg dw m^{-3}). The plants were uniformly placed on four shelves (3 m × 1.5 m each), 0.8 m above the ground. The entire shelf area was covered by the crop, corresponding to a canopy area of 18 m^2.

Three shelves were equipped with well-watered plants while the fourth one was equipped with plants under water restriction. Plants were normally watered twice a day (6 AM, 11 AM) by sub-irrigation using a complete nutrient solution. For plants under well-watered the water potential in the peat was maintained above -2 kPa, while the irrigation was periodically stopped on the fourth shelf until plants showed visual signs of water stress.

During the measurement period in June 2014, the leaf area index (LAI) was 2.36 m^2 m^{-2} for a plant density of 15 plants per m^2 and an average plant height of 240 mm. The leaf area was estimated by using a destructive method that consisted of cutting the leaves of four selected plants and determining the area of their leaves with an image analyser. Flowers were regularly removed during the experiment.

2.1.2 Microclimate measurements

A set of sensors was used to measure the climate characteristics inside and outside the greenhouse. Inside the greenhouse, only two shelves among the four available were equipped with different sensors, i.e., one shelf with plants under well-watered conditions and another one with plants under restricted water conditions; a schematic view of the experimental device is given in Fig. 1. The temperature (*Ta*) and relative humidity (*RHa*) of the air were measured by ventilated sensors (Vaisala HMP45C, Campbell Scientific Ltd., Antony, France; accuracy: ±0.1°C for T and ±2% for RH) located outside the greenhouse (*Ta_out, RHa_out*) and inside the greenhouse at 150 mm above the crop (*Ta1, RHa1*), and inside the crop (*Ta2, RHa2*). The measurements were made on two shelves, both for well-watered and restricted water conditions.

The ground temperature under the shelves (*Tw_g*), the temperatures of the lateral walls of the greenhouse (*Tw*) and the shade screen temperature (*Tsc*) were monitored with Pt100 probes (TC Online, France). The downward and the upward short and long wavelength radiations outside and inside the greenhouse were recorded by a CNR1 pyrradiometer (Kipp & Zonen, Delft, The Netherlands; accuracy: ±10%). The wind velocity outside the greenhouse was measured with a cup anemometer (HA 430A, ± 0.11 m s^{-1}; Geneq Inc., Canada)..All the above-mentioned parameters were measured every 3 seconds and averaged online over 10-min periods with a data logger system (CR3000 and CR7, Campbell Scientific Ltd., Antony, France).

2.1.3 **Shade screen and material properties**

Particular attention was paid to the modelling of the shade screen, with the aim of determining its radiative proprieties (i.e., refractive index and extinction coefficient). To reach this goal, preliminary steady-state simulations were conducted at 12 PM, and a range of values of the refractive index and extinction coefficient were tested until it was possible to correctly predict the measured temperature of the screen together with the measured short wave radiation just under the shade screen (312 K and 95 W m^{-2}, respectively, at 12 PM). On the basis of these preliminary simulations, values of 1.9 for the refractive index and 60 m^{-1} for the extinction coefficient were retained. With these values, a transmittance of 0.50 was obtained, which is very close to that given by (Montero, Anton, Biel, & Franquet, 1990), i.e., 0.45, for the same type of shade screen. Physical and thermal proprieties of the different materials involved in the studied system are provided in Table.1.

2.1.4 Substrate properties

The peat matric potential (Ψ, kPa) and volumetric water content (θ, v/v) were measured at mid-height inside six containers with six tensiometers (SDEC 1300, France;

accuracy: ±0.2% kPa), and six volumetric water content sensors (EC-5, Decagon, Dardilly, France; accuracy: ±3% m^3 m^{-3}). Three of them were placed inside well-watered containers and the other three inside restricted water containers. These parameters were also measured at 3-s intervals and averaged online over 10-min periods.

2.1.5 Plant activity

The temperatures of the leaves (T_l) at the top and the bottom of the crop were recorded at 3-second intervals with copper-constantan (Cu-Cs) thermocouples glued to the underside of three plant leaves at each position. The six measurements (three top and three bottom) were then averaged for the two positions over 10-min periods for each water condition. The stomatal resistance of the leaves was also measured using a porometer (AP4, Delta-T Device, Cambridge, UK). The accuracy of this device was ±20 s m^{-1} for R_s in the 20-50 s m^{-1} range, and ±10% in the 50-4000 s m^{-1} range. Five measurements were undertaken for green, young, healthy, fully-expanded leaves of different plants for each water condition and considering sunlit leaves. The measurements of R_s were replicated every half hour from 8 AM to 8 PM on selected days.

The amount of water lost by transpiration was measured with two high-resolution electronic scales (Melter-Toledo, Greifensee, Switzerland; capacity: 16 kg; accuracy: ±0.1 g) located under two shelves, approximately at the centre (Fig. 1), each one bearing six containers. One scale measured the transpiration of plants under well-watered conditions while the other one recorded the transpiration of plants under water restriction. Water loss was recorded every hour and the corresponding latent heat flux (Tr) was then expressed in W m^{-2} of ground area. Preliminary measurements showed that evaporation from the ground was negligible, meaning that transpiration could be assimilated to evapotranspiration.

2.2 Numerical modelling

The CFD simulations were carried out with the finite volume commercially-available CFD package, Ansys Fluent^{TM} 15 (ANSYS Inc., Canonsburg, PA, USA). This numerical tool solves the unsteady 2D Navier-Stokes conservation equations for mass (air and water vapour), momentum and energy. The interaction of plants with the microclimate, radiative transfers and the impact of substrate water content on transpiration were also included in the numerical tool. A 2D simulations approach was chosen, although 3D simulations are now widespread, for several reasons: (i) Many CFD studies of very specific mechanisms (ventilation, radiation, condensation) have been first conducted in 2D and then been transposed to 3D (Bournet & Boulard, 2010) because 2D makes it easier to assess specific mechanisms, and their coupling, by offering a better and easier control of the system. (ii) Most of the conducted 3D studies including a crop sub-model were undertaken under steady state conditions (Boulard, Roy, Pouillard, Fatnassi, & Grisey, 2017; Fatnassi, Boulard, Poncet, & Chave, 2006; Kichah et al., 2012b; Majdoubi et al., 2009). Only few study such as Nebbali et al. (2012) conducted a transient 3D study including a crop sub-model but without any validation. (iii) Validation of CFD models remains hard, due to the difficulty to map the parameters of interest (temperature, relative humidity, leaf temperature…) inside the whole building. (iv) Even if the power of computers continuously increases, the CPU time required to carry out transient 3D simulations remains prohibitive, CFD for 3D flow requires a greater number of discretization elements, and arranging a grid raises additional problems.

Conservation transport equations were solved using a second-order upwind discretization scheme to obtain better accuracy with a limited risk of divergence. A semi-implicit method for pressure-linked equations was adopted to solve the coupled pressure-momentum equations. The convergence criterion for all variables was 10^{-6}. The settings of the implemented CFD simulations are shown in Table 4.

2.2.1 Fundamental equations

Only two-dimensional cases were considered in this study because the prevailing flow rate was preferentially in a 2D plane perpendicular to the ridge as a consequence of the prevailing wind direction that was generally perpendicular to the vent openings. The transport equations may be written in the following general form (Eq. 1):

$$\frac{\partial \Phi}{\partial t} + \frac{\partial (U\Phi)}{\partial x} + \frac{\partial (V\Phi)}{\partial y} = \Gamma \Delta \Phi + S_{\Phi} \qquad (1)$$

where Φ represents the concentration of the non-dimensional transported quantity, namely momentum, mass (air and water vapour mass fraction) and energy; *U* and *V* are the components of the velocity vector; *Γ* is the diffusion coefficient; and S_{Φ} is the source term. The *k-ε* turbulence model (Launder & Spalding, 1974) was chosen as a closure model because it provided good agreement with experimental data in a number of studies for similar greenhouses (Bournet, Ould Khaoua, & Boulard, 2007; Nebbali et al., 2012). Air density depends not only on the temperature but also on the water vapour content in the air. Thus, the Boussinesq model cannot be applied, and the ideal gas law was used in order to link the fluid density to the other variables. The density was defined as a function of the temperature and mass fractions of the components of the mixture according to:

$$\rho = \frac{P_{op}}{RT \sum_i \frac{\omega_i}{M_i}} \qquad (2)$$

where *R* (= 8.31 J Mol^{-1} K^{-1}) is the universal gas constant, P_{op} (Pa) is the operating pressure, ω_i (kg kg^{-1}) is the mass fraction of species *i,* and M_i (kg mol^{-1}) is the molecular weight of species *i*.

2.2.2 Radiative sub-model

A radiative sub-model was activated in order to take account of the thermal contribution of radiative transfers and to serve as input for the transpiration sub-model. It distinguished the contribution of short [0.1 - 3 µm] and long wavelength radiation [3 - 100 µm] since the optical properties of the glass strongly depend on the wavelength band considered. The sub-model solves the equation of luminance for a finite number of discrete solid angles. The discrete ordinate (DO) method was chosen to calculate the radiation component since it proved to be efficient for comparable studies (Bournet et al., 2007; P.-E. Bournet & Boulard, 2010). The net contribution of radiation per unit volume in the energy equation was then calculated from the spatial integration of the monochromatic luminance over the whole wavelength spectrum. A full description of the bi-band model used in the present study may be found in Bournet et al. (2007). The canopy was considered as non-diffusive, meaning that only the direct fraction of the solar radiation was considered.

2.2.3 Crop sub-model

The crop was assimilated to a homogeneous porous medium made of a solid matrix with connected pores and creating a resistance to air movement. The crop exerted a mechanical strain onto the flow and interacted with the mass and energy balance of the air. The pressure loss induced by the crop resistance to air movement is represented in the Navier-Stokes equations using the Darcy-Forchheimer equation, as described by Kichah et al. (2012). The drag force per unit volume was expressed as a quadratic term of the velocity following Boulard and Wang (2002). The drag coefficient was estimated to 0.32, which, according to Kichah et al. (2012), is appropriate for an Impatiens crop According to these authors, the value of this coefficient appeared to be hardly affected by the hydric regime.

The energy balance along the leaves may be written as follows (Eq. 3):

$$Rg_{abs} - Tr_d - Q_s = 0 \qquad (3)$$

meaning that the canopy absorbed a radiation Rg_{abs} (W m^{-3}), which resulted from the solar radiation and exchanges caused by both a latent heat flux density Tr_d (W m^{-3}) by transpiration and a sensible heat flux density Q_s (W m^{-3}) with the ambient air. The absorbed radiation Rg_{abs} (W m^{-3}) in each cell of the canopy can be directly deduced from Beer's law, as described in Bouhoun Ali et al. (2018). The radiation extinction coefficient that appears in Beer's law was estimated from PAR radiation measurements above and below the canopy at a value of 0.95 for well-watered and 0.64 for restricted water conditions in this study. This difference was explained by the hydric stress signs that appeared on leaves for plants under water restriction as soon as the matric potential reached -10kPa. The sensible heat flux at the canopy level was determined by Eq. 4:

$$Q_s = 2 \cdot LAD \cdot \rho_a \cdot C_p \frac{T_l - T_a}{R_a} \tag{4}$$

where ρ_a is the air density (kg m^{-3}), C_p is the specific heat of air under constant pressure (J kg^{-1} K^{-1}), and T_l and T_a are the temperatures of leaves and air, respectively. The leaf temperature T_l was deduced from Eq. 5:

$$T_l = \frac{R_a}{2LAD\rho_a C_p}(Rg_{abs} - Tr_d) - T_a \tag{5}$$

The latent heat density (transpiration rate density) is given by Eq. 6:

$$\mathrm{Tr_d} = \frac{Rg_{abs} + 2\ \rho_a\ \mathrm{LAD}\ \mathrm{C_p}\ \mathrm{VPD_a}/\mathrm{R_a}}{\Delta + 2\ \gamma\left(1 + \frac{\mathrm{R_s}}{\mathrm{R_a}}\right)} \tag{6}$$

where γ is the psychrometric constant, $\mathrm{VPD_a}$ is the air-air vapour pressure deficit (Pa), and Δ is the slope of the saturated water vapour pressure curve according to temperature. In the present study, the aerodynamic resistance R_a was considered as constant according to (Baille, Baille, & Laury, 1994): $R_a = 271$ s m^{-1}. R_s is the stomatal resistance (s m^{-1}) calculated for each cell in the canopy domain. $\mathrm{R_s}$ was obtained from Bouhoun Ali, Bournet, Cannavo, Chantoiseau, & Sourgnes (2016) who used a Full Factorial Design method to determine the stomatal resistance from climatic and edaphic measurements according to Eq. 7:

$$R_s = \begin{pmatrix} -115 \cdot rg - 139 \cdot rh - 39 \cdot t + 139 \cdot rg \cdot rh + 43 \cdot rg \cdot t \\ +11 \cdot rh \cdot t \ + 661 \cdot rg^2 - 368 \cdot rg^3 \end{pmatrix} \cdot \left(1 + \left(\frac{\psi}{-11.41}\right)^{1.05}\right) \tag{7}$$

where rg = (Rg-75)/75; rh=(RHa-65)/10; t=(Ta-20.5)/5.5, and Ψ is the soil matric potential (kPa) deduced from the van Genuchten (1980) model (Eq. 8) given the soil water content θ (m^3 m^{-3}).

$$\psi = \left[\frac{1}{\alpha}\left(\frac{\theta-\theta_{res}}{\theta_{sat}-\theta_{res}}\right)^{\frac{N}{N-1}} - 1\right]^{1/N} \quad (8)$$

where θ_{res}, θ_{sat} are the residual and saturation soil volumetric water content (m^3 m^{-3}), and α (kPa^{-1}) and N (dimensionless) are the parameters to be calibrated. Using a multilinear fit, we found $\theta_{sat} = 0.887$ (m^3 m^{-3}), $\theta_{res} = 0.1$ (m^3 m^{-3}), $\alpha = 0.134$ (kPa^{-1}), and $N = 1.469$. Furthermore, the volumetric water content was calculated at each time step by integrating the transpiration and deduced from the initial volumetric water content (which depends on the initial amount of irrigation).

2.2.4 Mesh and boundary conditions

The calculation domain (29.40 × 10.15 m^2) was restricted to three greenhouse compartments to limit side effects, but only the central compartment including the shelves, the pots and the plants is analysed (Fig. 2). The total height of the plants was 330 mm, including the pots (90 mm), and the thickness of the shelf was 5 mm. A 2-mm-thick shade screen made of polyethylene and aluminium placed above the shelves was considered, with two chimneys of 250 mm tall on each side of the greenhouse, as well as 4-mm-thick glass walls.

An orthogonal structured mesh (151 × 330 cells) was retained for simulations with a refined grid in the vicinity of the ground and shelves, and a higher density in the area of the plants. The canopy consisted of 10 × 100 cells. Particular attention was paid to ensure the independence of the numerical results from the influence of the grid. After several attempts with different densities, a grid with 49,830 cells was chosen. It was a compromise between a dense grid that would require a long computational time, and a coarser grid that would have weakened the quality of the numerical results.

All boundaries conditions were established from the measurements provided by the different sensors (Fig. 1). The influence of external factors such as temperature, humidity and radiation was introduced through the boundary conditions as follows (Fig. 2):

(1) At the inlet section, a fixed velocity (average) was imposed using an average value (2 m s^{-1}) established from previous studies. The corresponding turbulent kinetic energy k in m^2 s^{-2} and dissipation rate profiles in m^2 s^{-3} at the inlet were calculated as a function of the friction velocity according to the formula established by Richards & Hoxey (1993). Uniform temperature (*Ta_out*) and absolute humidity (*AHa_out*) profiles obtained from the ventilated probe located outside the greenhouse were also imposed at the inlet boundary. The downward long wavelength radiative flux resulting from the emission of the atmospheric gases (e.g., water steam, carbonic gas and the ozone layer) was imposed through a sky temperature deduced from the long wavelength radiative flux measurements (Bournet et al., 2007). The sky temperature T_{sky} is defined as the temperature of the equivalent black body (emissivity = 1) that absorbs the same thermal radiation as the sky.

(2) Fixed temperatures were imposed for all lateral walls (*Tw*). Values were inferred from measurements at mid-height of walls (Fig. 1).

(3) Wall-type boundary conditions were used along the ground where a standard logarithmic wall function was imposed. The time series of temperature (*Tw_g*) and humidity, recorded at ground level, were also used to impose the corresponding boundary conditions.

(4) Along the upper limit of the calculation domain, downward short and long wave

radiations (Rg_out, R_{atm}_out) were imposed. Only downward short-wave radiation with a direction perpendicular to the upper limit was considered since it was assumed that the shade screen totally diffused the solar radiation, meaning that the solar direction had almost no impact on the resulting short wave radiation distribution under the screen. A slipping wall-type condition with no shear was also set at the upper limit, meaning that no mass transfer was allowed through this surface.

(5) At the outlet section, a pressure outlet condition was imposed, requiring the specification of a static pressure at the outlet boundary (P = 101,325 Pa), together with the infrared radiation (same value as the one retained for the inlet). All other flow quantities were extrapolated from the interior, corresponding to zero normal gradients.

The shelves were taken as grey bodies with an equivalent emissivity of 0.1, chosen in order to take account of the absorption capacity of the crop covering the shelves. The emissivity of the ground (which consists of concrete) was fixed to 0.5. Furthermore, the shade screen was considered to be a fully diffuse solid semi-transparent medium and was assumed to be a solid medium instead of a porous medium. This is because it was not possible to integrate the reflected part of the incident radiation for a porous medium with the latest version of Fluent and, in the present case, it was established that the reflected part of the incident radiation on the shade screen was the most important one. The thermal conductivity of the shade screen was taken as the thermal conductivity of polyethylene, i.e., 0.15 W m^{-1} K^{-1}, because it consisted primarily of polyethylene (84% compared with 16% of aluminium).

The model was run under unsteady-state conditions, meaning that the boundary conditions were re-actualized at each time step, and the field of variables calculated at the previous time step was used as the initial conditions for the current time step. To define the right time step, we tested several time step sizes (10 min and 1 h) and observed almost no difference for results at a given instant. This means that a solution at a given time is rather independent from the solution at the previous time step, but mainly the consequence of the evolution of the boundary conditions. Consequently, a 1 h time step was retained for simulations.

2.3 Case study

The model was first validated against data recorded inside the experimental greenhouse under clear sky conditions, distinguishing two irrigation strategies: the first case consisted of well-watered plants, while the second one consisted of restricted water plants. For both cases, 2D unsteady simulations over a 23-hour period with a 1-hour time step were carried out from 11 pm on June 17th to 10 pm on June 18th, 2014. The irrigation was stopped on June 13th for plants under water restriction. The experimental climatic measurements were used as input data for the initial and boundary conditions (Figs. 3A, 3B). Initial conditions at 11 pm were obtained by running a preliminary simulation using the boundary conditions recorded at 10 pm and assumed to be uniformly distributed over the whole calculation domain.

The initial peat water content was 0.870 $m^3 m^{-3}$ (i.e., peat water field capacity at Ψ = -1 kPa) for well-watered plants, whereas it was equal to 0.652 $m^3 m^{-3}$ for plants under water restriction. A sub-model based on the water balance was used (Eq. 5) to calculate the soil matric potential at each time step. For the well-watered case, the soil matric potential was considered as constant and its value was fixed at -1 kPa.

The evolution of the boundary conditions used for the simulation is provided in Fig. 3. Data were recorded every 10 min and averaged over 1-h periods. As expected, for both water regimes, the evolution of the boundary conditions revealed a correlation between the global radiation and the temperature, with a peak of temperature at around 2 pm.

2.4 Statistical analysis

To estimate the difference between the simulated variables for the different irrigation regimes and the simulated variables for the reference case, the gap between the considered irrigation case *j* and the reference case $\mathrm{D}_{ref,j}$ given by Eq. 9 was calculated for each variable together with the cumulated transpiration ratio (CTR) (i.e., cumulated *Tr* for a given irrigation regime divided by the cumulated *Tr* of the reference):

$$\mathrm{D}_{ref,j} = \sqrt{\frac{1}{k}\sum_1^k \left(\mathrm{y}_{ref,i} - y_{j,i}\right)^2} \tag{9}$$

where $y_{ref,i}$ is the variable for the reference case at time step *i*, $y_{j,i}$ is the variable for an irrigation regime of *j* % at time step *i*, and *k* is the total number of data inputs.

3 RESULTS AND DISCUSSION

3.1 Model validation

Validation of the model was undertaken both for well-watered plants and for plants under water restriction considering a first case with only well-watered plants and a second case with only plants under water restriction. Temperature, humidity and plant properties including stomatal resistance and transpiration rates were considered for comparison with experimental data.

3.1.1 Temperature

The time evolutions of the air temperatures at two locations and the average leaf temperatures for well-watered and restricted water conditions are shown in Figs. 4A, 4B, 5A and 5B. Both measured and predicted air temperatures inside and above the crop and leaf temperatures followed the same trend. The order of magnitude of the predicted temperatures was in fair agreement with measurements for both water regimes (Table 3). For well-watered plants, r^2 (coefficient of determination) > 0.91 and RMSE < 1.56 K for all temperatures. Similar results were found for temperatures for plants under restricted water conditions, with r^2 higher than

0.86 and RMSE lower than 1.87 K (Table 3). Temperatures were quite well predicted above the canopy for both regimes, as shown in Figs; 4A and 4B. It may be noted, however, that around solar midday, simulated air temperatures above the canopy were almost 1 K higher for the restricted water conditions than for well-watered ones, whereas measurements disclosed similar temperatures for both cases. This is mainly due to the fact that for the simulations, only one type of plants (i.e. well-watered or under water restriction) was considered inside the greenhouse compartment, whereas for measurement purposes, the greenhouse contained both types of plants. Thus, the air temperature above the canopy in the experimental greenhouse was mainly influenced by well-watered plants. The effect of water restriction can be better seen on measured and predicted temperatures inside the canopy and on the leaf temperatures with values in well-watered conditions greater by up to 1 K to 2 K compared with plants under well-watered conditions, as indicated in Figs. 5A and 5B. As expected, the transpiration cooled the leaves of plants and refreshed the adjacent air. Water restriction limited transpiration and, as a result, the cooling effect almost vanished. Indeed, it can be seen that the measured and predicted temperatures for the leaves were lower than the temperature of the air inside the canopy during daytime for the well-watered case (Fig. 5A). This difference became very small in the case of water restriction (Fig. 5B) since the transpiration rate was too low to cool the leaves.

As mentioned before, particular care was paid to correctly simulate the shade screen. When comparing the measured and simulated temperatures of the screen for both well-watered and restricted water conditions, only a small difference was reported with RMSE of less than 3 K for temperatures within the 287-315 K range, and an $r^2 > 0.95$ was found for both regimes (Fig. 6). A thorough analysis shows that during the daytime, simulated temperatures were in good agreement with measured ones for both regimes, whereas simulated temperatures were greater at night. This difference probably stems from the fact that the shade screen was considered as a solid medium instead of a porous medium. As a consequence, mass flow through the screen was not simulated and convective heat transfer through the screen was only limited to transfers through the two lateral chimneys. Simulations also show that the impact of water restriction on the screen temperature was negligible (Fig. 6).

3.1.2 Humidity

The relative humidity was studied at two locations for both regimes, as was done for temperature. The time evolution of the measured and predicted relative humidity is plotted in Figs. 7A and 7B. As expected, the predicted and measured *RH* were higher inside the canopy than in the air just above, especially for the well-watered case. For the restricted water case, the measured and predicted humidity above and inside the canopy remained similar because of the decrease of the transpiration rate (explained below) and the higher temperature inside the canopy compared with the well-watered case. In general, acceptable agreement was found between measured and calculated humidity for both water regimes. However, the model overestimated the humidity inside the canopy (*RHa2*) mainly for the restricted water case. This could be due to the fact that since the simulated shade screen was considered as not being porous, it prevented the air from flowing through, thus limiting the evacuation of water vapour outside the greenhouse. The following results were obtained for all relative humidity: $r^2 > 0.94$ and RMSE < 10% for well-watered plants, and $r^2 > 0.78$ and RMSE < 6.69% for the restricted water case (Table 3). Good agreement between measured and simulated soil matric potential was also found with $r^2 = 0.99$ and RMSE = 0.32 kPa for the restricted water case.

3.1.3 Plant properties

a. Stomatal resistance

The CFD model again showed its ability to correctly predict the time evolution of the stomatal resistance R_s throughout the day for sunlit leaves and for both regimes (Figs. 8A and

8B) with RMSE = 133.58 s m^{-1} and r^2 = 0.48 for the well-watered case. For the case of water restriction, RMSE=389.12 s m^{-1} and r^2=0.45 were obtained. Furthermore, as shown in Figs. 8A and 8B, measured and predicted R_s for the restricted water case were higher than R_s for the well-watered case, for sunlit leaves. These differences were clearly related to the irrigation regime. The stomatal resistance (Fig. 8B) increased (from about 10-11 am) to limit the transpiration when the soil matric potential decreased and the extraction of available water from the substrate became more difficult (Verhoef & Egea, 2014). Similar behavior was reported for well-watered plants (Fig. 8A), but to a far lesser extent. In that case, the evolution of R_s was instead linked to the evolution of the global radiation and the air-to air-vapour pressure deficit.

b. Transpiration

As expected, the measured and simulated transpirations for the restricted water case (Fig. 9B) were lower than the ones for the well-watered case (Fig. 9A). Globally, the model demonstrated its ability to correctly predict the time evolution of the transpiration rate with good accuracy for both regimes: r^2 = 0.98 and RMSE = 9.92 W m^{-2} for the well-watered case, and r^2 = 0.98 and RMSE = 3.50 W m^{-2} for the restricted water case. The relative error for accumulated transpiration over 23 h was also estimated, leading to an underestimation by the model of 11.40% for the well-watered case and of 5.12% for the restricted water case.

Simulations also revealed heterogeneities in the transpiration rate distribution both for the well-watered and restricted water cases inside the canopy, generally from the top to the bottom of the canopy, as shown in Figs. 10A and 10B. The distribution of transpiration was strongly dependent on the global radiation distribution over the canopy height, with high values at the top and a decrease toward the bottom. Also, as mentioned earlier, the lower the stomatal resistance was, the higher the transpiration rate was, and the stomatal resistance itself was lower for higher values of global radiation. This fact also partly explains why transpiration rates of sunlit leaves at the top of the canopy were higher than that of the shaded leaves inside and at the bottom of the canopy.

3.2 Test of different irrigation scenarios

Once the model was validated, it was used to test a set of irrigation scenarios, with the aim to assess the behaviour of the plants in response to different levels of water restriction. The idea was to identify to what extent water inputs could be reduced without really impacting plant transpiration and, subsequently, plant activity in general.

Six irrigation regimes were tested and a reference case was chosen corresponding to a 100% irrigation regime, i.e., to a substrate retention capacity of 0.870 m^3 m^{-3}. This value was set as an initial condition inside the substrate at the beginning of the simulation at 10 pm. For the other irrigation regimes, the amount of initial water content was reduced by using 90% of the water supply compared to the reference case (0.783 m^3 m^{-3}), 80% (0.696 m^3 m^{-3}), 70% (0.609 m^3 m^{-3}), 60% (0.522 m^3 m^{-3}) and 50% (0.435 m^3 m^{-3}). The radiation extinction coefficient was fixed at 0.95 for cases when the peat matric potential was greater than -10 kPa and at 0.64 for cases when it was lower than -10 kPa as reported from former measurements of the PAR distribution inside the canopy. A first 1-h simulation was initiated at 10 pm using the boundary conditions described in Figs. 2 and 3 and assuming that all of the variables were uniformly distributed over the whole calculation domain at that time in order to obtain the initial conditions at 11 pm The simulations with 1-hour time steps were then carried out considering a 23-h period from 11 pm on June 17th to 11 pm on June 18th, 2014, with values for the boundary conditions also inferred from the same measurements used for the previous part (Figs. 2 and 3). As for the validation case, a one-hour time step was chosen for simulations.

Table 4 provides the main results obtained for the different irrigation scenarios. These results are analysed into details in the following sections.

3.2.1 Temperature

Table 4 compares restricted water cases with the reference case and shows the increasing impact of water restriction on air temperature just above the canopy (*Ta1*) as the surrounding air becomes warmer when water inputs are reduced. This trend increased inside the canopy for *Ta2*. For the leaf temperature T_l, the temperature difference with the reference case also increased with water restriction. The difference between the leaf temperatures and the adjacent air temperatures may be used as an indicator of plant water stress (González-Dugo, Moran, Mateos, & Bryant, 2006; Jackson, Idso, Reginato, & Pinter, 1981). Indeed, with the decrease of the water supply, the amount of water evacuated by transpiration decreased until it became too low to cool the leaves, as described below. The results of the average difference between *Tl* and *Ta2* calculated for each irrigation regime clearly showed that the gap between the air temperatures inside the canopy and leaf temperatures was reduced with the increase in water restriction until the leaf temperatures became greater than the neighbouring air temperature. This type of situation occurred when the water supply was reduced by more than 30%: *Tl* became higher than *Ta2* by 0.5 K (Table 4), leading to plant water stress. A threshold value of 0.5 K difference in temperature between leaves and air (scenarios 60% and 50%) was considered as the criterion for discussing plant stress. As for the 70% scenario, a positive average of difference (*Tl*-*Ta2*) of 0.2 K close to the temperature probe accuracy could hardly be detected by this one and could therefore not be considered as significant. Indeed, for the comfort of the plant, it is preferable to keep the temperature of the leaves (*Tl*) lower, or almost equal to, the temperature of the adjacent air (*Ta2*) (Gonzalez-Dugo, Zarco-Tejada, & Fereres, 2014).

The temporal evolutions of the simulated air temperatures at two locations above and inside the canopy (refer to Fig. 1) and simulated leaf temperatures for the six irrigation regimes are shown in Fig. 11. These temperatures followed the same trend for all irrigation regimes with a bell shape of the temperature curves. Nevertheless, they slightly increased when the water supply was reduced. For instance, for a 50% water supply, the air temperatures above and inside the canopy, as well as the leaf temperatures, could be up to 4 K, 5 K and 3 K greater than the reference case, respectively. This may be explained by the fact that a modification of the water regime strongly impacted the transpiration rate, i.e., the latent heat transfer, and, consequently, the energy balance over the canopy.

A comparison between the leaf and air temperatures inside the canopy for the different irrigation regimes was also undertaken to assess the effect of water restriction on the transpiration process. For the well-watered conditions corresponding to the reference case, the leaf temperatures in the middle of the day were smaller than the adjacent air temperatures simulated inside the canopy at location 2 (referring to Fig. 1). Indeed, plant transpiration cooled the leaves of plants and, consequently, refreshed the adjacent air. This cooling process was reduced for lower transpiration rates until the leaf temperatures became greater than the neighbouring air temperature, which happened from the 90% scenario but became significant (> 0.5°C) from the 60% scenario.

3.2.2 Humidity

The predicted time evolution of the relative humidity is plotted in Fig. 12 for the six irrigation scenarios. As expected, the relative humidity was higher inside the canopy than in the air just above or below the canopy. This is particularly true for the reference case. As the restriction degree increased, the humidity decreased at both locations because of the decrease in the transpiration rate and the higher temperatures inside the canopy.

This decrease is quantified for each irrigation regime in Table 4. Since it is known that high humidity levels could create favourable conditions for fungal diseases like botrytis (Bartzanas, Boulard, & Kittas, 2004), the reduction of the water supply could provide a partial solution to this problem.

To provide a general idea of the relative humidity distribution inside the greenhouse compartment, humidity contours for three irrigation regimes are plotted in Fig. 13 (Reference, 70% and 50%). Here again, humidity distributions were almost similar for the reference case and the 70% irrigation scenario. Above the screen, humidity was mainly determined by the outside humidity of the air flow entering the greenhouse. With the increase in water restriction (50% scenario) lower values of humidity were predicted not only in the area located between the screen and the shelf, but also inside the canopy and under the shelves.

3.2.3 Peat matric potential

The predicted peat matric potential evolution according to the water irrigation scenario is presented in Fig. 14. The peat matric potential decreased with decreasing water supply, reaching a minimal value of nearly -65 kPa for the 50% water supply scenario. It was considered that stress began when the matric potential reached -10 kPa, and the permanent wilting point (i.e., plant death) occurred when it was lower than -100 kPa (Gobat, Aragno, & Mattey, 2004). In the present study, irrigation scenarios did not make it possible to reach the permanent wilting point. Nevertheless, for cases for which the water supply was less than 80% of the reference, the -10 kPa threshold was reached, so it could be considered that water stress was only obtained for lower water content scenarios. As expected, it was also predicted that the greatest decrease in the growing media matric potential for a given irrigation regime occurred during the day as a consequence of the higher transpiration activity of the plants.

3.2.4 Plant properties

a. Stomatal resistance

As also reported in the validation stage, the decrease in water supply caused an increase in R_s (Fig. 15). Indeed, the progressive closure of stomatal apertures limited plant transpiration as the growing medium matric potential decreased (Fig. 14), meaning that the extraction of available water from the substrate had become more difficult (Verhoef & Egea, 2014). However, once the soil water potential was higher than -10 kPa (considering the threshold reported by (Cannavo et al., 2016)), the stomatal resistance of the sunlit leaves was almost in the same range (96-1141 s m^{-1}) with no significant difference, regardless of the irrigation regime (see Figs. 14 and 15). For these water potentials, it may thus be deduced that the transpiration activity of the plant will be maintained at a level comparable to the reference case (well-watered). The minimal stomatal resistance simulated for each irrigation regime was found to be barely affected by water restriction except when it dropped to lower than 70% of the reference case (Table 4).

b. Transpiration

Not surprisingly, predicted transpiration rates (Fig. 16) decreased with lower water inputs. From the reference 100% to 60% of the water supply, little reduction on plant transpiration was predicted. Greater differences appeared when the water supply was reduced by 50%.

The cumulated transpiration ratios (CTR) between a given irrigation scenario and the reference are provided in Table 4, showing a progressive decrease in the transpiration rate while the stomata apertures were closing, following a reduction in water input. This trend was not linear and increased for high water depletion.

The distribution of transpiration inside the crop also revealed heterogeneities mainly associated with the non-homogeneous distribution of R_s (Fig. 15) throughout the canopy. The leaves located near the ground of the crop had the lowest transpiration rates and, conversely, the highest transpiration rates were simulated at the top of the crop. The transpiration distributions were almost the same for the reference case (Fig. 17a) and 70% of the water supply (Fig. 17b), whereas for the 50% water supply scenario (Fig. 17c), distributions were very different from the reference case with far lower *Tr* values. However, the horizontal distribution of the transpiration rates seemed to be barely impacted by the horizontal heterogeneity in air velocity and humidity inside the canopy, meaning that the radiation distribution was probably the main factor affecting the transpiration rate.

4 CONCLUSION

The aim of this study was to investigate crop transpiration inside a greenhouse compartment, focusing on cases for which plants were under water restriction. To reach this goal, an unsteady CFD model was implemented that included an adapted crop sub-model that took the water balance inside the substrate-plant-atmosphere continuum into account. The CFD model showed its ability to correctly predict the evolution of the soil matric potential, microclimatic temperatures and plant transpiration both for well-watered and restricted water regimes. The model also correctly predicted the differences between both regimes: the measured and simulated air temperatures inside the canopy and leaf temperatures were higher for the restricted water conditions than for the well-watered case. Also, and as expected, the measured and simulated transpiration rates were lower for the plants under water restriction than for the plants under well-watered conditions.

In a second step, the effect of six water regimes on plants and the microclimate under greenhouse conditions was studied. The CFD model made it possible to quantify the impact of the different irrigation regimes on the air temperature, relative humidity above and inside the canopy, leaf temperatures, growing media matric potentials, stomatal resistances and transpiration rates. Conclusions similar to those obtained for the validation stage were addressed concerning the evolution of temperature and relative humidity.

Hence, CFD simulations could be helpful to improve water management strategy making it possible to preserve the microclimate conditions adapted to plant development while reducing water inputs. To avoid stomatal closure (which would reduce photosynthesis activity) and maintain transpiration activity, the leaf temperatures should remain close to the adjacent air temperatures during the day. From that point of view, the scenario with 70% water supply appears to be a good compromise. Moreover, using 70% of water instead of 100% makes it possible to save 0.19 l per container and per day. In addition to spare water, another advantage of reducing water supply is that it contributes to decrease humidity and therefore risks of fungal diseases or mould development.

Nevertheless, the impact of water restriction on plant architecture should also be investigated to ensure that the plants will remain marketable. Furthermore, the model still needs improvements to better predict plant interaction with the local climate conditions. Thus, it will be interesting to investigate the impact of water restriction on photosynthetic activity by including the CO_2 cycle inside the model. Eventually, in the next stage, 3D simulations will be implemented to assess the distribution of climatic and plant variables and increase the realism of the model.

ACKNOWLEDGEMENTS

This study was carried out within the EPHor Research Unit at Agrocampus Ouest, in Angers, France. The authors would like to thank the Premier Tech Company for providing the peat, and D. Lemesle and D. Renard, who performed the laboratory measurements. Experiments were conducted at the ImHorPhen (shared experimental facilities) with the assistance of R. Gardet.

List of tables

Table 1. Material proprieties.

Table 2. Settings of the CFD simulations.

Table 3. Coefficients of determination and root mean square errors calculated for the air and leaf temperatures (*Ta1*, *Ta2*, *Tsc* and T_l) and for relative humidity (*RHa1* and *RHa2*).

Table 4. Results of the simulations for the six irrigation scenarios tested.

List of figures

Fig. 1. Experimental setup with the different sensors used: ventilated sensors for temperatures and relative humidities outside the greenhouse (*Ta_out*; *RHa_out*), and above (*Ta1*; *RHa1*) and inside (*Ta2*; *RHa2*) the canopy; *CNR1* to measure radiation outside and inside the greenhouse; thermocouples: for leaf (*Tl*), walls (*Tw*), shade screen (*Tsc*), ground (*Tw_g*); anemometer to measure the wind velocity and scales to quantify the transpiration rate. "*w*": west; "*e*" east; "*c*": measurements on well-watered plants (comfort); "*r*": measurements on restricted water plants.

Fig. 2. Calculation domain and boundary conditions.

Fig. 3. Time evolution of the boundary conditions for a compartment within a greenhouse with Impatiens plants. A: ground temperature (*Tw_g*), air temperature (*Ta_out*), west wall temperature (*Tw_w*), east wall temperature (*Tw_e*). B: long wave radiation (*Ratm_out*); short wave radiation (*Rg_out*); air absolute humidity (*AHa_out*) (n= 6).

Fig. 4. Time evolution of measured and simulated air temperatures above the crop (*Ta1*), for well-watered plants "*c*" (A) and for plants under restricted water "*r*" conditions (B).

Fig. 5. Time evolution of measured and simulated air temperature inside the crop (*Ta2*) and average leaf temperatures (*Tl*), for well-watered plants "*c*" (A) and for plants under restricted water "*r*" conditions (B).

Fig. 6. Time evolution of measured and simulated shade screen temperatures (*Tsc*) for well-watered plants (A) and for plants under restricted water conditions (B).

Fig. 7. Time evolution of measured and simulated relative humidities above (*RHa2*) and inside (*RHa1*) the crop, for well-watered plants (A) and for plants under restricted water conditions (B).

Fig. 8. Time evolution of measured and simulated stomatal resistance of sunlit leaves for plants under well-watered (A) and restricted water (B) conditions.

Fig. 9. Time evolution of measured and simulated transpiration rates for plants under well-watered (A) and restricted water (B) conditions.

Fig. 10. Representation of the area assigned to the crop within the CFD domain where a distribution of the crop transpiration rate (W m^{-2}) was simulated inside the canopy domain at 12 pm on June 18th, 2014, for well-watered (A) and restricted water (B) conditions.

Fig. 11. Time evolution of simulated air temperatures above (*Ta1*) and inside (*Ta2*) the crop, and average leaf temperatures (T_l), for the different irrigation regimes.

Fig. 12. Time evolution of simulated relative humidity above (*RHa1*) and inside (*RHa2*) the canopy for the different irrigation regimes.

Fig. 13. Distributions of relative humidity inside the greenhouse compartment with a crop at 12 PM for three irrigation scenarios; ref.: 100% (a); 70% (b); and 50% (c).

Fig. 14. Time evolution of simulated peat matric potential for different irrigation regimes.

Fig. 15. Time evolution of simulated stomatal resistance of sunlit leaves for different irrigation regimes.

Fig. 16. Time evolution of simulated transpiration rates for different irrigation regimes.

Fig. 17. Simulated distribution of the crop transpiration rate (W m^{-2}) at 12 pm on June 18th, 2014, for plants under 100% water supply (a), 70% (b) and 50% (c).

References

Baille, M., Baille, A., & Laury, J. C. (1994). A simplified model for predicting evapotranspiration rate of nine ornamental species vs. climate factors and leaf area. *Scientia Horticulturae*, *59*(3–4), 217–232. https://doi.org/10.1016/0304-4238(94)90015-9

Bartzanas, T., Boulard, T., & Kittas, C. (2004). Effect of Vent Arrangement on Windward Ventilation of a Tunnel Greenhouse. *Biosystems Engineering*, *88*(4), 479–490. https://doi.org/10.1016/j.biosystemseng.2003.10.006

Bouhoun Ali, H. B., Bournet, P.-E., Cannavo, P., Chantoiseau, E., & Sourgnes, M. (2016). Stomatal resistance of New Guinea Impatiens pot plants. Part 1: Model development for well watered plants based on design of experiments. *Biosystems Engineering*, *149*, 112–124.

Bouhoun Ali, H., Bournet, P.-E., Cannavo, P., & Chantoiseau, E. (2018). Development of a CFD crop submodel for simulating microclimate and transpiration of ornamental plants grown in a greenhouse under water restriction. *SI: CFD in Agri.Bio.Eng.*, *149*, 26–40. https://doi.org/10.1016/j.compag.2017.06.021

Boulard, T., & Wang, S. (2002). Experimental and numerical studies on the heterogeneity of crop transpiration in a plastic tunnel. *Computers and Electronics in Agriculture*, *34*(1–3), 173–190. https://doi.org/10.1016/S0168-1699(01)00186-7

Boulard, Thierry, Roy, J.-C., Pouillard, J.-B., Fatnassi, H., & Grisey, A. (2017). Modelling of micrometeorology, canopy transpiration and photosynthesis in a closed greenhouse using computational fluid dynamics. *Biosystems Engineering*, *158*, 110–133. https://doi.org/10.1016/j.biosystemseng.2017.04.001

Bournet, P. E., Ould Khaoua, S. A., & Boulard, T. (2007). Numerical prediction of the effect of vent arrangements on the ventilation and energy transfer in a multi-span glasshouse using a bi-band radiation model. *Biosystems Engineering*, *98*(2), 224–234. https://doi.org/10.1016/j.biosystemseng.2007.06.007

Bournet, P.-E., & Boulard, T. (2010). Effect of ventilator configuration on the distributed climate of greenhouses: A review of experimental and CFD studies. *Computers and Electronics in Agriculture*, *74*(2), 195–217.

Cannavo, P., Bouhoun Ali, H., Chantoiseau, E., Migeon, C., Charpentier, S., & Bournet, P.-E. (2016). Stomatal resistance of New Guinea Impatiens pot plants. Part 2: Model extension for water restriction and application to irrigation scheduling. *Biosystems Engineering*, *149*, 82–93. https://doi.org/10.1016/j.biosystemseng.2016.07.001

Fatnassi, H., Boulard, T., Poncet, C., & Chave, M. (2006). Optimisation of Greenhouse Insect Screening with Computational Fluid Dynamics. *Biosystems Engineering*, *93*(3), 301–312. https://doi.org/10.1016/j.biosystemseng.2005.11.014

González-Dugo, M. P., Moran, M. S., Mateos, L., & Bryant, R. (2006). Canopy temperature variability as an indicator of crop water stress severity. *Irrigation Science*, *24*(4), 233–240.

Gonzalez-Dugo, V., Zarco-Tejada, P. J., & Fereres, E. (2014). Applicability and limitations of using the crop water stress index as an indicator of water deficits in citrus orchards. *Agricultural and Forest Meteorology*, *198–199*, 94–104. https://doi.org/10.1016/j.agrformet.2014.08.003

Jackson, R. D., Idso, S. B., Reginato, R. J., & Pinter, P. J. (1981). Canopy temperature as a crop water stress indicator. *Water Resources Research*, *17*(4), 1133–1138.

Kichah, A., Bournet, P.-E., Migeon, C., & Boulard, T. (2012). Measurement and CFD simulation of microclimate characteristics and transpiration of an Impatiens pot plant crop in a greenhouse. *Biosystems Engineering*, *112*(1), 22–34. https://doi.org/10.1016/j.biosystemseng.2012.01.012

Launder, B. E., & Spalding, D. B. (1974). The numerical computation of turbulent flows. *Computer Methods in Applied Mechanics and Engineering*, *3*(2), 269–289. https://doi.org/10.1016/0045-7825(74)90029-2

Majdoubi, H., Boulard, T., Fatnassi, H., & Bouirden, L. (2009). Airflow and microclimate patterns in a one-hectare Canary type greenhouse: An experimental and CFD assisted study. *Agricultural and Forest Meteorology*, *149*(6–7), 1050–1062. https://doi.org/10.1016/j.agrformet.2009.01.002

Monteith, J.L. (1977). Resistance of a partially wet canopy: Whose equation fails? *Boundary Layer Meteorol.*, *12*, 375–383.

Montero, J. I., Anton, A., Biel, C., & Franquet, A. (1990). Cooling of greenhouses with compressed air fogging nozzles. *Acta Horticulturae*, 199–210. https://doi.org/10.17660/ActaHortic.1990.281.22

Nebbali, R., Roy, J. C., & Boulard, T. (2012). Dynamic simulation of the distributed radiative and convective climate within a cropped greenhouse. *Renewable Energy*, *43*, 111–129. https://doi.org/10.1016/j.renene.2011.12.003

Richards, P. J., & Hoxey, R. P. (1993). Appropriate boundary conditions for computational wind engineering models using the k-ϵ turbulence model. *Journal of Wind Engineering and Industrial Aerodynamics*, *46*, 145–153.

Van Genuchten, M. Th. (1980). A closed-form equation for predicting the hydraulic conductivity of unsaturated soils. *Soil Science Society of America Journal*, *44*, 892–898.

Verhoef, A., & Egea, G. (2014). Modeling plant transpiration under limited soil water: Comparison of different plant and soil hydraulic parameterizations and preliminary implications for their use in land surface models. *Agricultural and Forest Meteorology*, *191*, 22–32. https://doi.org/10.1016/j.agrformet.2014.02.009

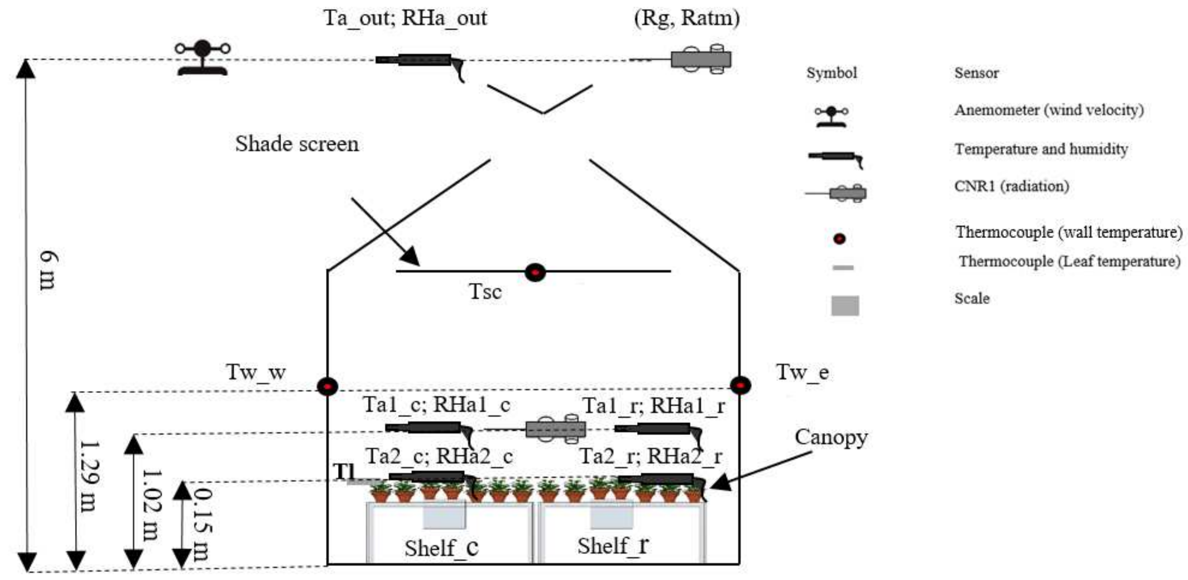
Ta_out; RHa_out
(Rg, Ratm)
Shade screen
Tsc
6 m
Tw_w
Tw_e
Ta1_c; RHa1_c
Ta1_r; RHa1_r
Ta2_c; RHa2_c
Ta2_r; RHa2_r
Canopy
Tl
1.29 m
1.02 m
0.15 m
Shelf_c
Shelf_r
Symbol
Sensor
Anemometer (wind velocity)
Temperature and humidity
CNR1 (radiation)
Thermocouple (wall temperature)
Thermocouple (Leaf temperature)
Scale

Figure 1

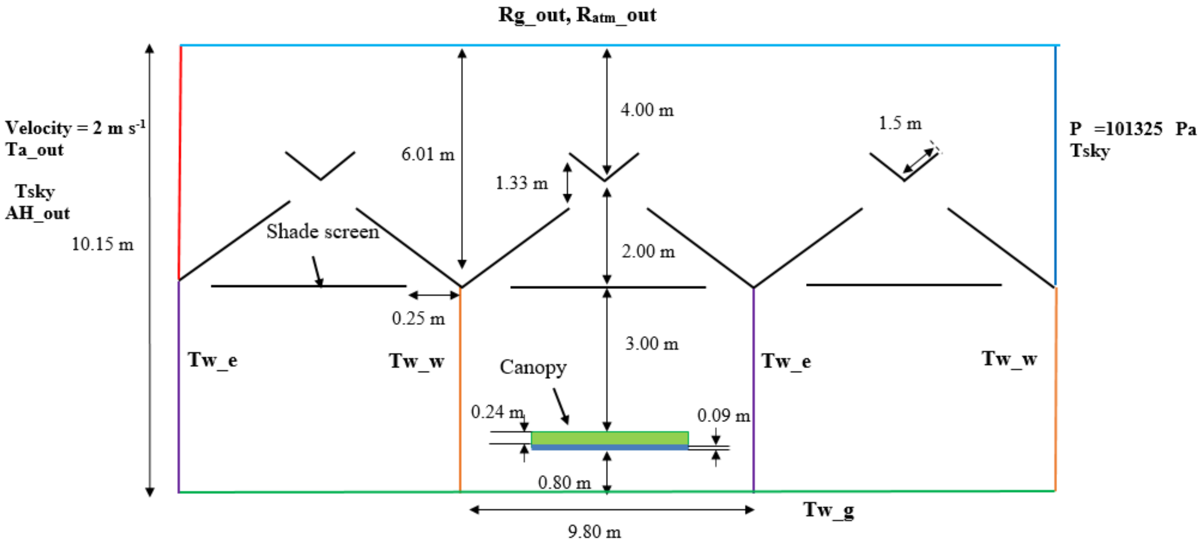
Rg_out, Ratm_out
Velocity = 2 m s-1
Ta_out
Tsky
AH_out
10.15 m
6.01 m
4.00 m
1.33 m
1.5 m
P =101325 Pa
Tsky
Shade screen
2.00 m
0.25 m
3.00 m
Tw_e
Tw_w
Canopy
Tw_e
Tw_w
0.24 m
0.09 m
0.80 m
Tw_g
9.80 m

Figure 2

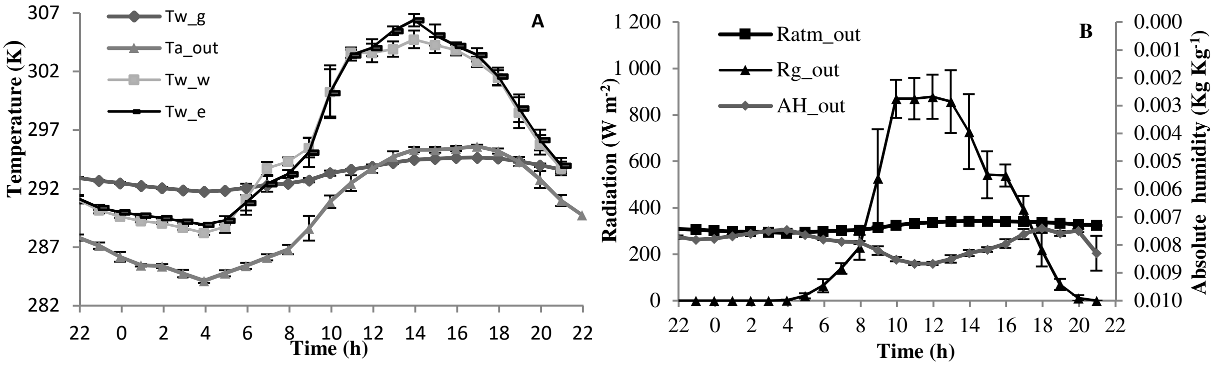
A
Temperature (K)
307
302
297
292
287
282
Tw_g
Ta_out
Tw_w
Tw_e
22 0 2 4 6 8 10 12 14 16 18 20 22
Time (h)
B
Radiation (W m^{-2})
1 200
1 000
800
600
400
200
0
Ratm_out
Rg_out
AH_out
Absolute humidity (Kg Kg^{-1})
0.000
0.001
0.002
0.003
0.004
0.005
0.006
0.007
0.008
0.009
0.010
22 0 2 4 6 8 10 12 14 16 18 20 22
Time (h)

Figure 3

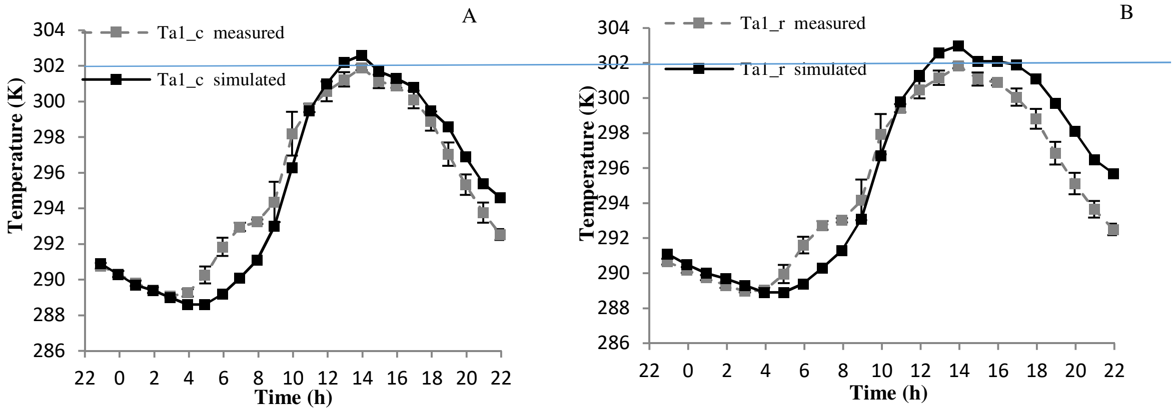
A
Ta1_c measured
Ta1_c simulated
Temperature (K)
304
302
300
298
296
294
292
290
288
286
22 0 2 4 6 8 10 12 14 16 18 20 22
Time (h)
B
Ta1_r measured
Ta1_r simulated
Temperature (K)
304
302
300
298
296
294
292
290
288
286
22 0 2 4 6 8 10 12 14 16 18 20 22
Time (h)

Figure 4

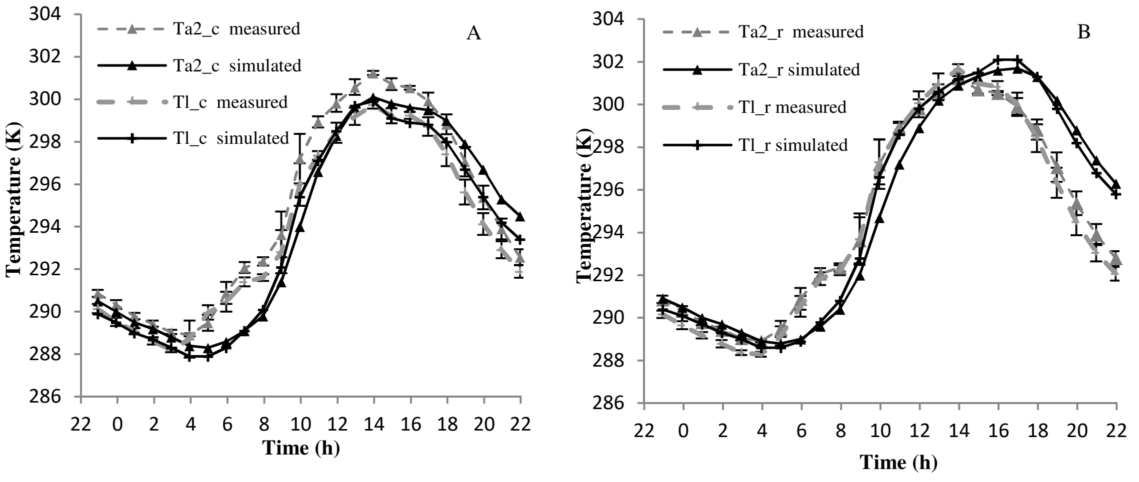
A
Ta2_c measured
Ta2_c simulated
Tl_c measured
Tl_c simulated
Temperature (K)
Time (h)
304
302
300
298
296
294
292
290
288
286
22
0
2
4
6
8
10
12
14
16
18
20
22
B
Ta2_r measured
Ta2_r simulated
Tl_r measured
Tl_r simulated
Temperature (K)
Time (h)

Figure 5

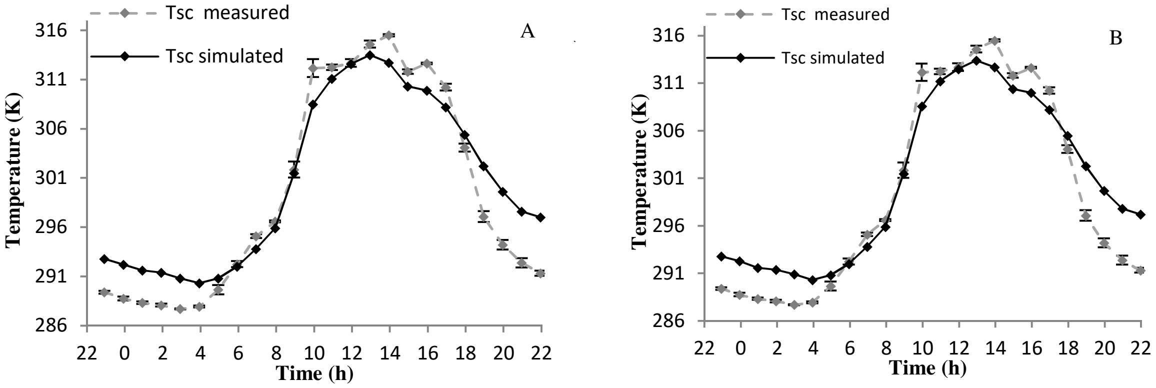
Tsc measured
Tsc simulated
A
B
Temperature (K)
316
311
306
301
296
291
286
Time (h)
22
0
2
4
6
8
10
12
14
16
18
20
22

Figure 6

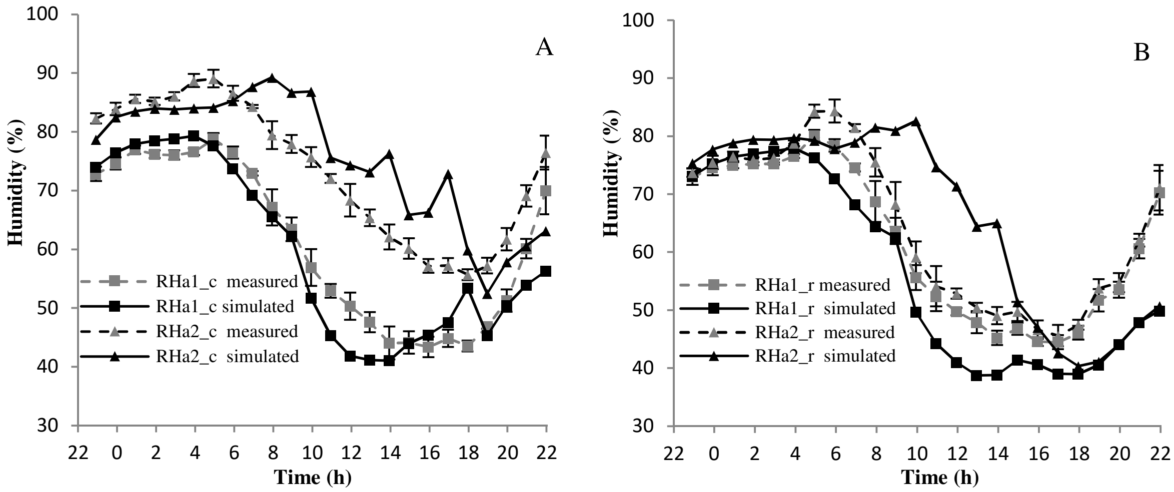
A
Humidity (%)
100
90
80
70
60
50
40
30
22
0
2
4
6
8
10
12
14
16
18
20
22
Time (h)
RHa1_c measured
RHa1_c simulated
RHa2_c measured
RHa2_c simulated
B
Humidity (%)
Time (h)
RHa1_r measured
RHa1_r simulated
RHa2_r measured
RHa2_r simulated

Figure 7

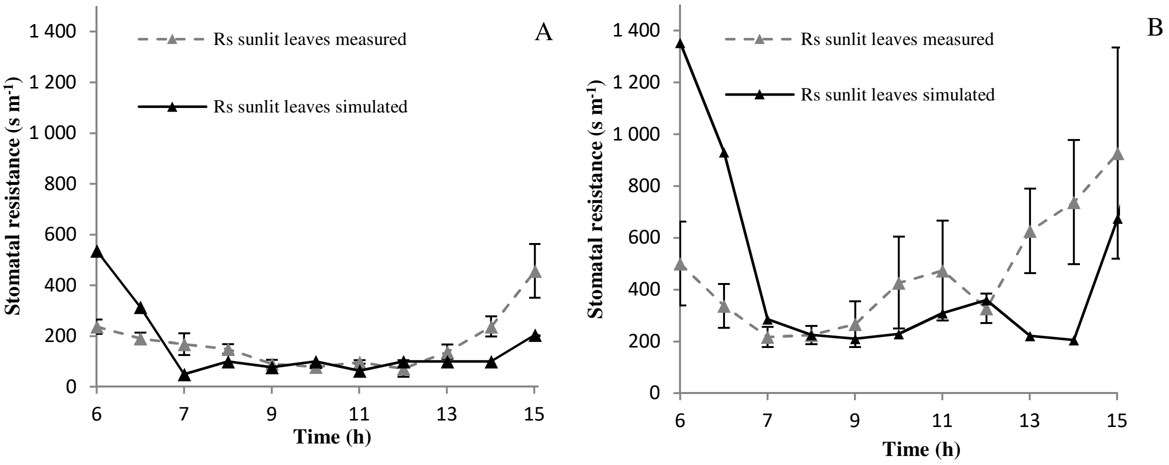
A
B
Rs sunlit leaves measured
Rs sunlit leaves simulated
Stomatal resistance (s m^{-1})
1 400
1 200
1 000
800
600
400
200
0
6
7
9
11
13
15
Time (h)

Figure 8

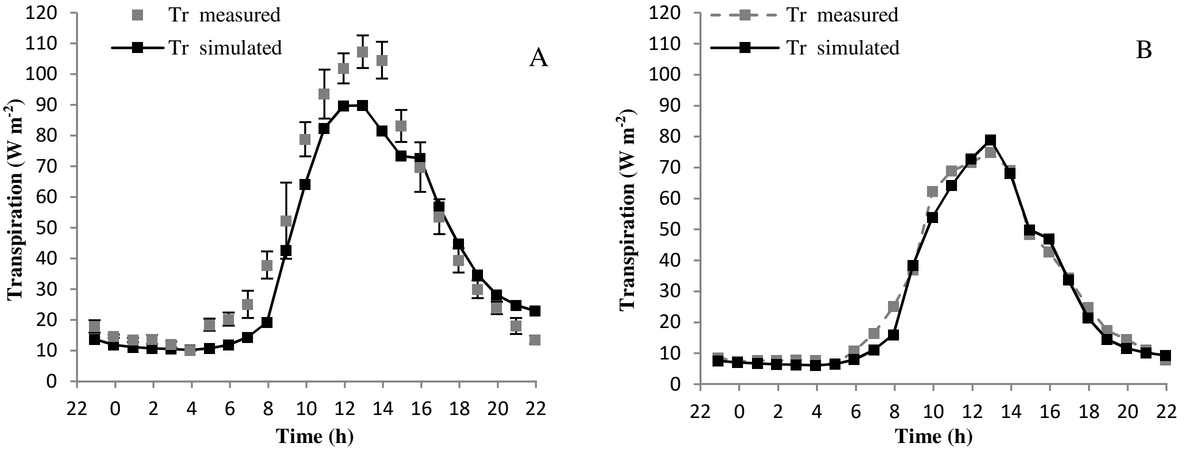
Transpiration (W m^{-2})
120
110
100
90
80
70
60
50
40
30
20
10
0
Tr measured
Tr simulated
A
22 0 2 4 6 8 10 12 14 16 18 20 22
Time (h)
B

Figure 9

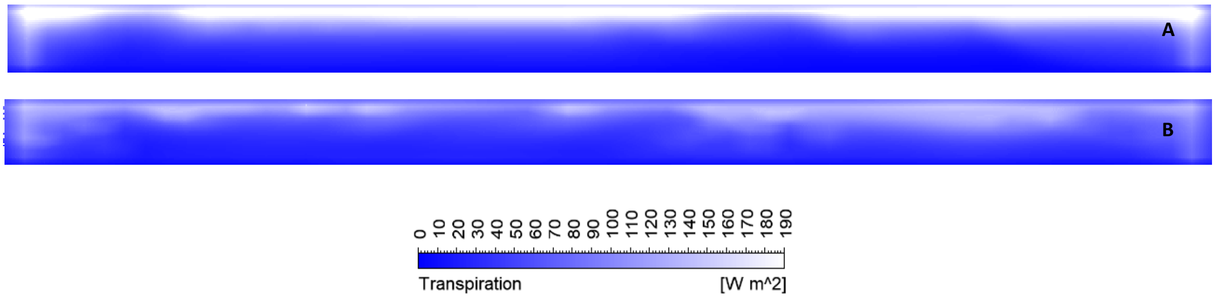
A
B
0 10 20 30 40 50 60 70 80 90 100 110 120 130 140 150 160 170 180 190
Transpiration
[W m^2]

Figure 10

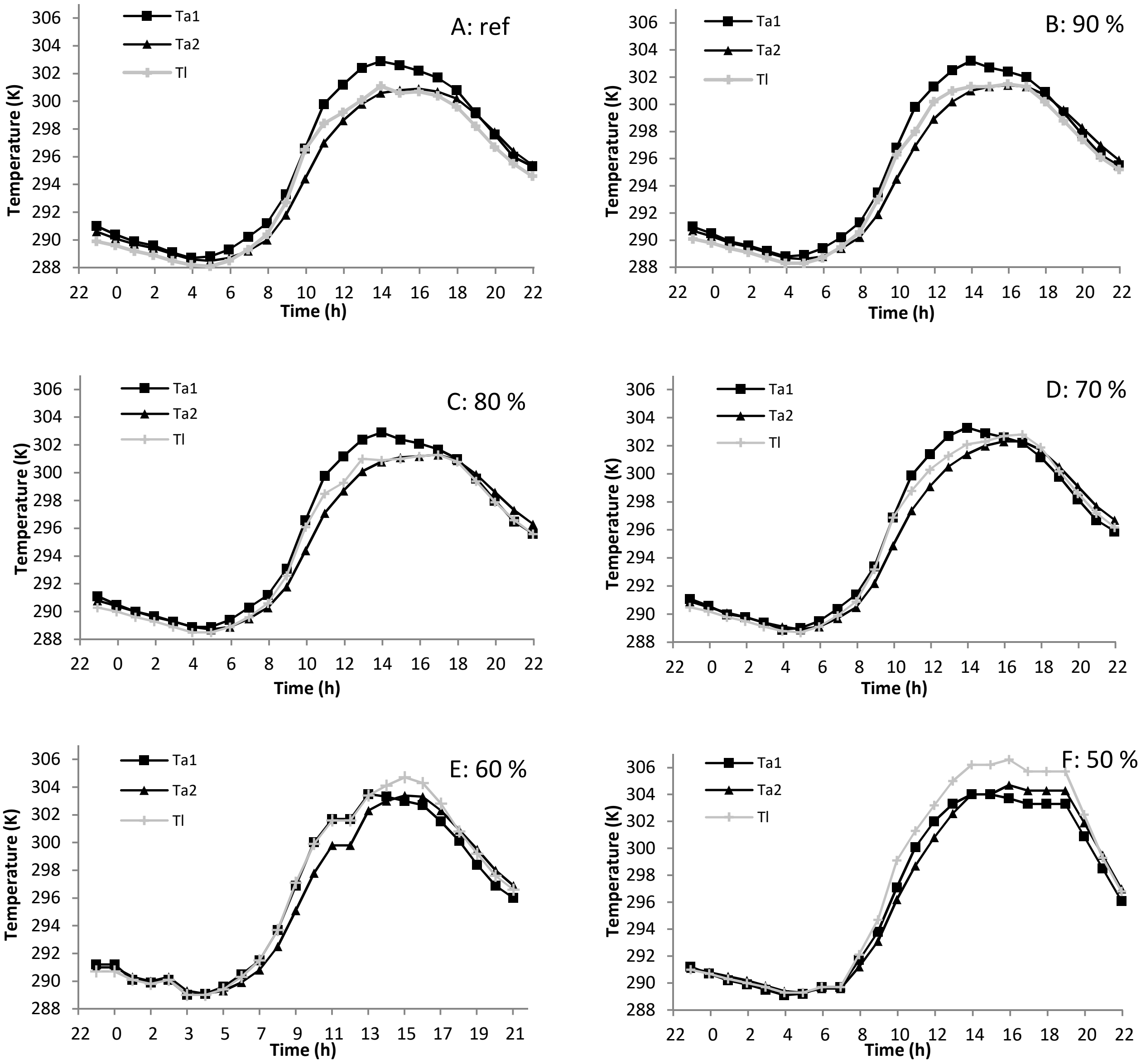A: ref
B: 90 %
C: 80 %
D: 70 %
E: 60 %
F: 50 %
Ta1
Ta2
Tl
Temperature (K)
Time (h)
306
304
302
300
298
296
294
292
290
288
22
0
2
4
6
8
10
12
14
16
18
20
22
3
5
7
9
11
13
15
17
19
21

Figure 11

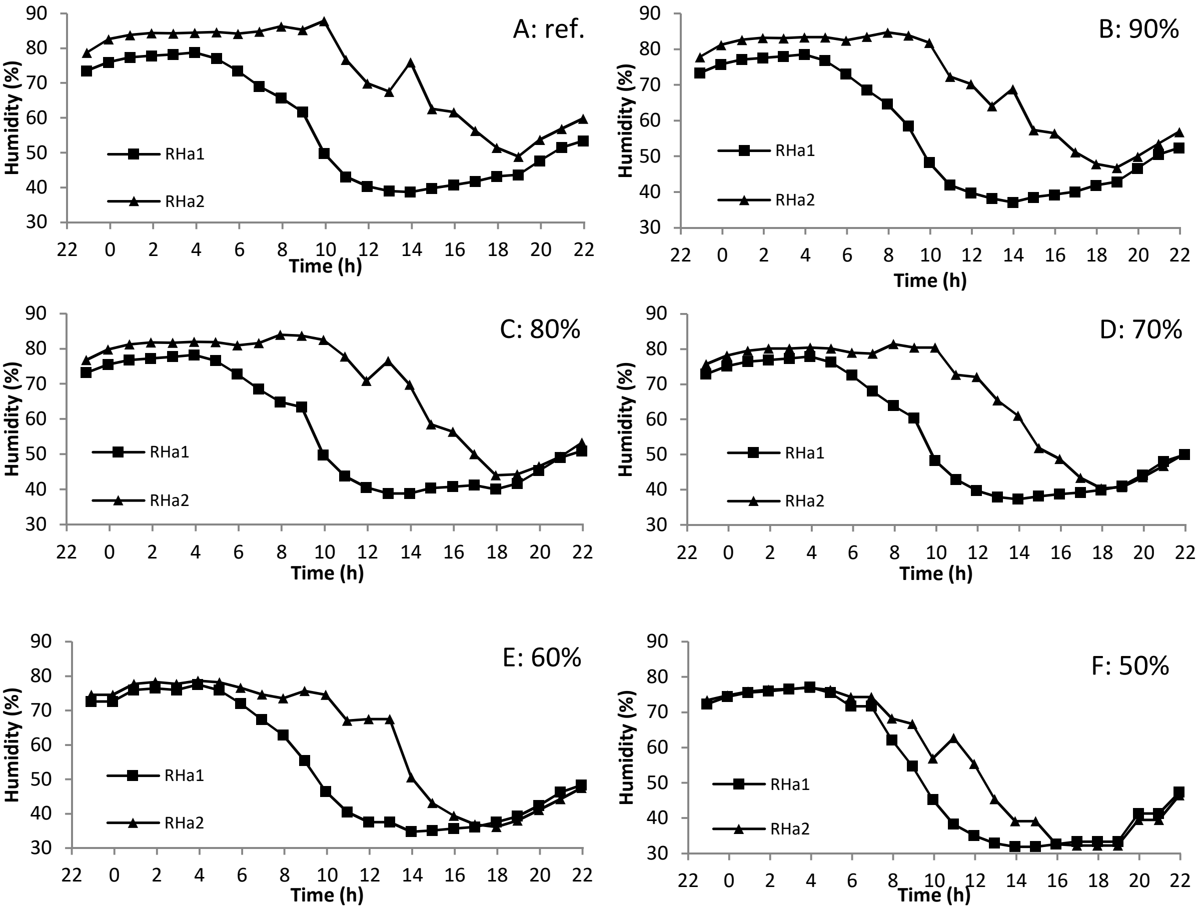

A: ref.
B: 90%
C: 80%
D: 70%
E: 60%
F: 50%
Humidity (%)
Time (h)
RHa1
RHa2
90
80
70
60
50
40
30
22
0
2
4
6
8
10
12
14
16
18
20
22

Figure 12

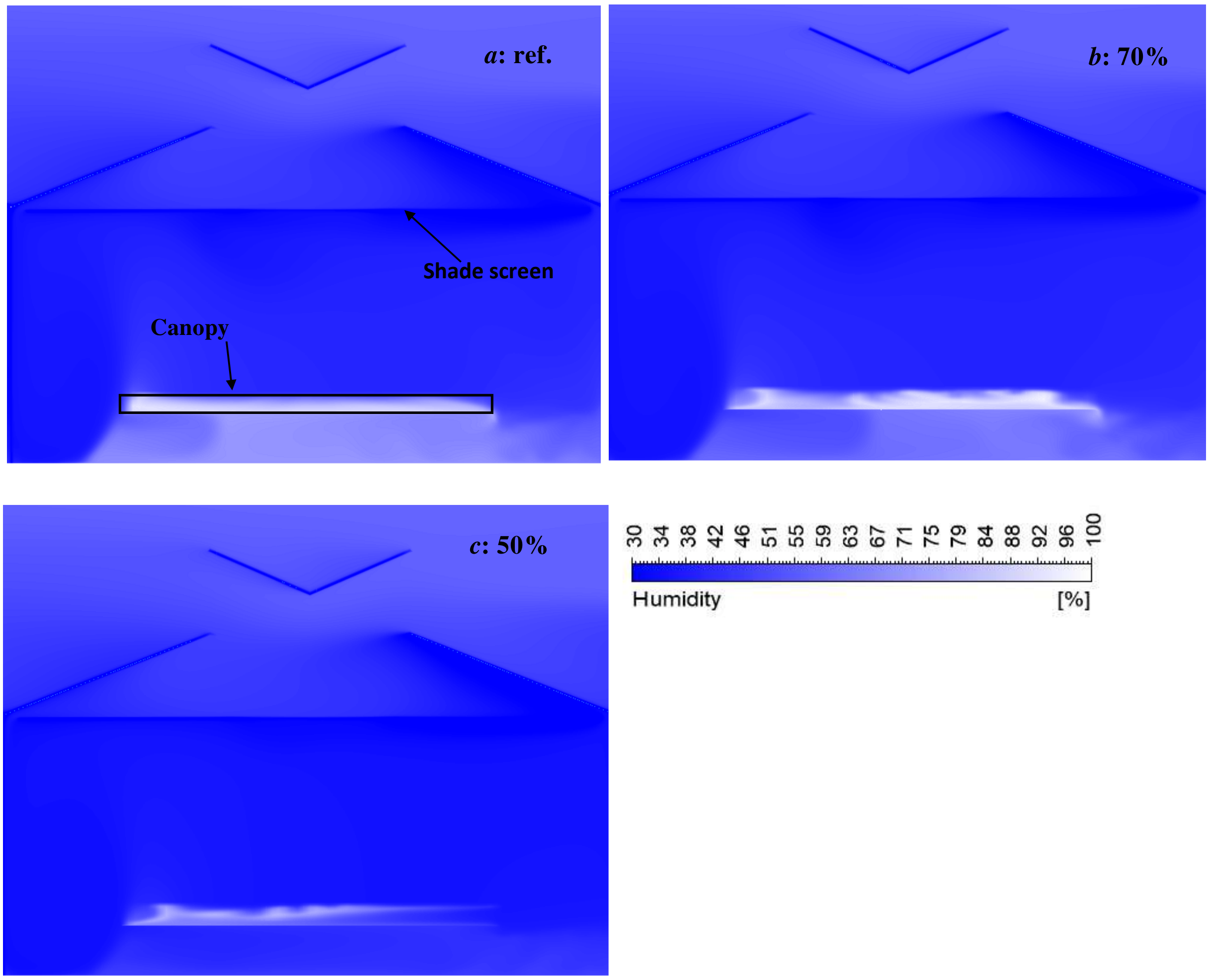
a: ref.
Shade screen
Canopy
b: 70%
c: 50%
30 34 38 42 46 51 55 59 63 67 71 75 79 84 88 92 96 100
Humidity
[%]

Figure 13

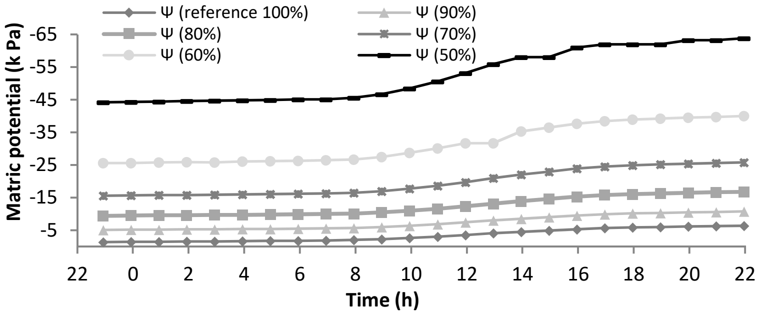
Ψ (reference 100%)
Ψ (90%)
Ψ (80%)
Ψ (70%)
Ψ (60%)
Ψ (50%)
Matric potential (k Pa)
-65
-55
-45
-35
-25
-15
-5
22
0
2
4
6
8
10
12
14
16
18
20
22
Time (h)

Figure 14

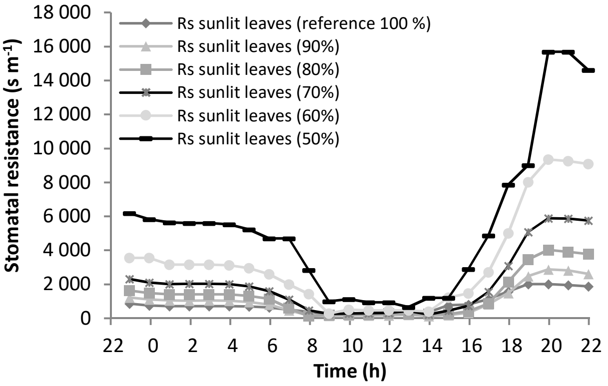
Rs sunlit leaves (reference 100 %)
Rs sunlit leaves (90%)
Rs sunlit leaves (80%)
Rs sunlit leaves (70%)
Rs sunlit leaves (60%)
Rs sunlit leaves (50%)
Stomatal resistance (s m-1)
18 000
16 000
14 000
12 000
10 000
8 000
6 000
4 000
2 000
0
22
0
2
4
6
8
10
12
14
16
18
20
22
Time (h)

Figure 15

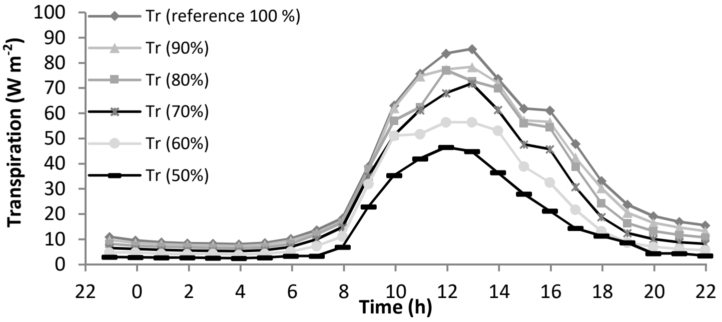

Transpiration (W m^{-2})
100
90
80
70
60
50
40
30
20
10
0
22
0
2
4
6
8
10
12
14
16
18
20
22
Time (h)
Tr (reference 100 %)
Tr (90%)
Tr (80%)
Tr (70%)
Tr (60%)
Tr (50%)

Figure 16

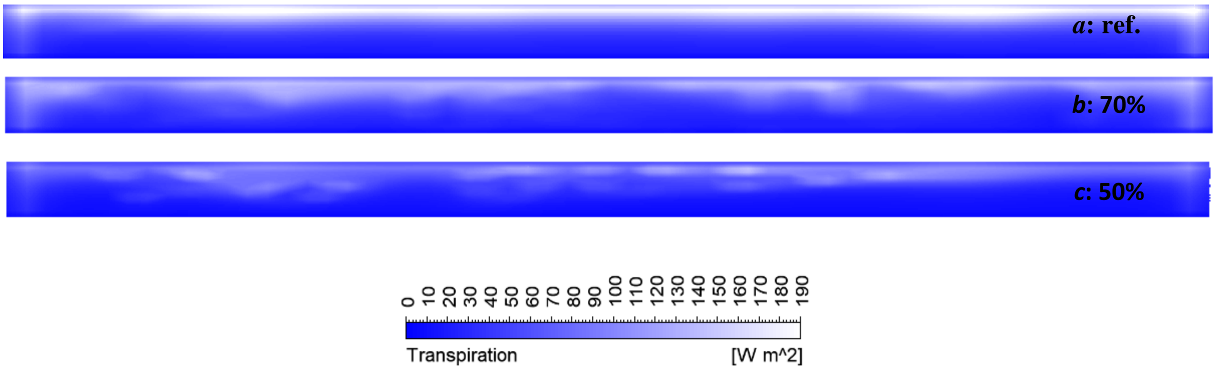
a: ref.
b: 70%
c: 50%
0
10
20
30
40
50
60
70
80
90
100
110
120
130
140
150
160
170
180
190
Transpiration
[W m^2]

Figure 17

Table 1

Location (material)	Layer(s) thickness, mm	Density (kg m^{-3})	Specific heat (J K^{-1} kg^{-1})	Thermal conductivity (W m^{-1} K^{-1})	Refractive index	Emissivity
Roofs, Walls (glass)	4	2500	800	800	1.52	0.9
Shelves (aluminum)	5	2719	871	202.4	-	0.1
Shade screen	2	940	2260	0.15	1.9	0.1
Soil (concrete)	1000	2300	2300	202.4	-	0.5
Air	-	1.22	1006	0.0242	1	-
Water vapour	-	0.554	f(T)	0.0261	1	-

Table 2

CFD component	Setting
Solver	2D Pressure based algorithm Simple scheme pressure-velocity coupling 2nd order implicit upwind scheme for spatial and time discretization standard scheme for pressure discretization
Density	Ideal gas law to compute density
Turbulence	Standard k-ε Standard wall functions
Radiation	DO (discrete ordinates) Theta divisions: 10 Iterations ratio (flow/radiation): 10
Species model	Mixture (air and water vapour)
Relaxation factors	0.3 for water vapour, kinetic energy, dissipation rate, turbulent viscosity 0.5 for DO, energy, pressure, density, body forces, momentum
Convergence criteria	10^{-6} for continuity, velocity, kinetic energy, dissipation rate, energy, water vapour mass fraction, radiation
Cells number	151*330
Time step size	1h
Number of time steps	23
Iterations per time step	1500

Table 3

Case study	**Parameter**	**Ta1 (K)**	**Ta2 (K)**	**Tsc (K)**	**T_l (K)**	**RHa1 (%)**	**RHa2 (%)**
Well-watered	r^2	0.94	0.91	0.95	0.95	0.98	0.94
	RMSE	1.34	1.56	3.01	1.04	4.99	9.97
Water restriction	r^2	0.92	0.86	0.95	0.89	0.91	0.78
	RMSE	1.69	1.87	3.06	1.83	6.69	9.76

Table 4

Irrigation scenario/ Simulated quantity	**Ref. (100%)**	**90%**	**80%**	**70%**	**60%**	**50%**
$D_{ref,j}$(Ta1 [K])		0.16	0.20	0.35	0.61	1.33
$D_{ref,j}$(Ta2,i [K])		0.34	0.45	0.89	1.37	2.37
Average T_l-Ta2 [K]	-0.10	0.01	0.02	0.22	0.52	0.92
$D_{ref,j}$(RHa1,i [%])		1.12	1.29	1.87	3.72	5.89
$D_{ref,j}$(RHa2,i [%])		3.37	4.74	7.58	12.42	18.05
Cumulated transpiration CTR [%]		93	86	75	61	44